Semicond. Sci. Technol. **15** (2000) 277–285. Printed in the UK PII: S0268-1242(00)09367-6

Microscopic analysis of the influence of Ge profiles on the current-noise operation mode of n-Si/p-$Si_{1-x}Ge_x$ heterostructures

M J Martín, D Pardo and J E Velázquez

Departamento de Física Aplicada, Universidad de Salamanca, Plaza de la Merced s/n, 37008 Salamanca, Spain

E-mail: mjesus@rs6000.usal.es

Received 8 November 1999, accepted for publication 12 January 2000

Abstract. A comparative Monte Carlo study dealing with the influence of the Ge profile on current-mode operation noise of n-Si/p-$Si_{1-x}Ge_x$ heterojunctions is presented. Uniform profiles with different Ge contents ($x = 0$, 0.15, 0.3) as well as graded profiles of Ge in the p region are considered. We focus on the alteration of stationary carrier transport and on the microscopic origin of high-frequency noise through different factors such as the transport in the pseudomorphic SiGe layer, band discontinuities in Ge box-profile heterojunctions or the electric field due to Ge grading. Our microscopic study shows that a Ge box profile produces larger enhancement in electron current density than in graded profiles. However, the triangular Ge profile produces the best noise characteristics of the devices studied throughout the considered frequency range. Regarding the low-frequency values of noise equivalent temperature, T_n, our study shows that the SiGe/Si heterojunctions provide lower values of T_n than the Si homojunction within the current density range. Under low-injection conditions the Ge grading leads to a striking reduction in T_n.

1. Introduction

Increasingly in this age, the requirements of low-cost solutions for frequencies at or above 1 GHz for RF and microwave circuit applications demand the development of new technologies. Owing to the possibility of using silicon–germanium, SiGe, alloys to implement bandgap engineering in Si systems, silicon technologies are now beginning to enter a market formerly occupied by GaAs field-effect transistor technology. The advantage of SiGe heterojunction bipolar transistors (HBTs) [1, 2] over III–V HBTs is that the exceptionally advanced Si production line can be used in SiGe technology with only a modest increase in process complexity retaining excellent values of common-emitter dc-current gain (β) and transition frequencies (f_T) [3]. As a direct consequence of bandgap discontinuity between Si and SiGe, the HBT allows a dramatic increase in the base doping without degrading β and hence a reduction in both base resistance and base width. Therefore, using these devices, the low noise figures required in modern communication systems can be achieved [4], highlighting the potential of SiGe HBTs.

Transistor noise performance becomes an important issue in RF and microwave systems in which low-frequency noise ($1/f$) exerts a fundamental limit. Owing to their vertical transport characteristics SiGe HBTs exhibit excellent $1/f$ noise performance [5]. In addition, high-frequency noise of the transistor plays a major role in system sensitivity since it sets the signal-to-noise level. Within this frequency range an important type of noise is the *thermal* noise, which is generated by mechanisms that are intrinsic to the random nature of carrier transport, and therefore establish a lower noise limit for all semiconductor devices. Nevertheless other microscopic processes such as generation–recombination mechanisms, carrier mass and mobility change between both sides of the junction due to band discontinuities and strain, fluctuations in barrier height, . . . are also responsible for noise in an HBT.

A microscopic-based noise analysis seems to be a promising and powerful tool for characterizing and improving high-speed and low-noise SiGe HBT technology. The Monte Carlo method self-consistently coupled to a Poisson solver [6] was chosen for our purpose because the different noise sources are intrinsically included in the simulations [7–11]. This procedure was used in previous studies about the origin of the current fluctuations in silicon bipolar homojunctions [10]. Further, the physical interpretation of the total current fluctuations in terms of the electron, hole and crossed (electron–hole and hole–electron) fluctuations was performed. More recently, a preliminary evaluation of the effect of strained SiGe layers on current noise in n-SiGe/p-Si heterojunctions was presented [12].

Prior to an accurate and complex two-dimensional

study of an n-Si/p-SiGe/n-Si HBT, in the present work the physical origin of high-frequency noise phenomena in the heterojunction n-SiGe/p-Si is undertaken. Instead of a two-dimensional model for a bipolar transistor, a 1D model is used because it can successfully simulate the device behaviour [13]. The features of our 1D bipolar Monte Carlo simulator in relation to the physical model of the strained SiGe layer on Si and to the handling of the Si/SiGe heterojunction have been described in detail elsewhere [12, 14].

This paper is organized in the following manner. In section 2 we describe the devices studied. The study is comparative and the structures examined have the same geometry and doping profiles while the Ge molar fraction and profile vary. The aims of the work are developed in sections 3 and 4. Section 3 focuses on the alteration of stationary carrier transport through different issues such as transport in the pseudomorphic SiGe layer, valence and conduction band discontinuities at the junction, ΔE_c and ΔE_v respectively, and the electric field due to Ge grading. Our findings agree with the well known effects of heterojunctions on the diode forward current and serve as a solid basis for the ensuing part of this work. In section 4, we attempt to gain insight into the microscopic origin of the high-frequency noise. A method based on considering a spatial analysis of current fluctuations on the Si and SiGe layers of bipolar heterostructures has recently been presented [12]. Using this spatial analysis we determine the combined effects of the pseudomorphic SiGe layer and different Ge profiles on the noise characteristics of n-Si/p-$Si_{1-x}Ge_x$ heterostructures. A discussion of the low-frequency value of equivalent noise temperature is also examined for both box and triangular Ge profiles. The conclusions of this work are summarized in section 5.

2. Simulated structures

The simulated structures are all formed by a 0.3 μm n^+-type Si region with an uniform doping level of 10^{23} m^{-3} and a 0.4 μm p-type SiGe region with a constant doping profile of 5×10^{21} m^{-3} and different Ge profiles. As long as doping levels and geometry are the same as those in a pn homojunction published previously, it is possible to conduct a comparative study to pinpoint the influence of Ge profile on noise behaviour. In our particular case, the SiGe layer is assumed to be strained in spite of its thickness surpassing the critical thickness [15] in order to compare the results obtained for the different heterostructures with those obtained previously for a silicon device [10]. Accordingly, our structures can be comparable to the emitter–base junctions of ideal bipolar transistors [16]. Figure 1 shows the Ge profile and the band diagram of the n-Si/p-$Si_{1-x}Ge_x$ heterostructures studied. Different Ge contents (x_{Ge}) were considered for the p region (figure 1): in the first structure it is formed by silicon (H1). In the second and the third structure we considered a uniform or box Ge profile with x_{Ge} equal to 0.15 (H2) and 0.3 (H3). The leading edge of the constant Ge profile is the metallurgical n–p junction generating ΔE_c and ΔE_v at this spatial position [17, 18]. In H2 or H3, the electrons encounter a weak spike at the heterointerface in the conduction band, CB, when moving from the n^+ region to the p region while the SiGe side is a potential well for the holes.

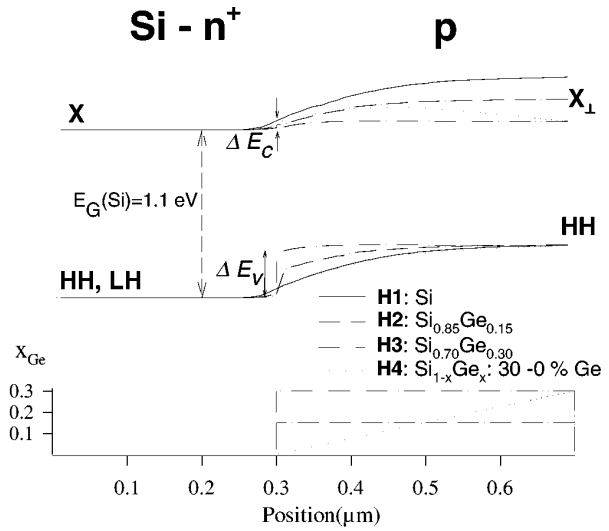

Figure 1. Germanium profile, x_{Ge}, of the Si/SiGe structures together with the band diagram under forward-bias conditions of the SiGe-p–Si-n^+ structures. Note that X and $X_\perp$ ([100] and [010] valleys) constitute the minimum of the CB in Si and in strained SiGe on [001] Si, respectively [19]. The usual degenerate heavy-hole (HH) and light-hole (LH) sub-bands are shifted in SiGe on [001] Si, where the HH becomes the maximum of the VB.

In the fourth structure, H4, the Ge content is linearly graded (triangular profile) across the p region from $x_{Ge} = 0.0$ in the n–p junction to $x_{Ge} = 0.3$ at the end of the p region. At both sides of the heterostructures ohmic contacts are located and the treatment of the carriers flowing through the contacts has been described in detail in [10, 19].

The differences between the graded SiGe heterojunction and the other structures are best illustrated by using the energy band diagram shown in figure 1. On the one hand, on comparing the band structures of abrupt and graded heterojunctions one sees that the Ge grading across the p region produces a smooth spatial variation in the CB and VB (valence band) edges, consequently, eliminating the energy spikes or notches in both bands, whose existence would retard the diffusion and drift of the minority carrier through this SiGe layer. On the other hand, the x_{Ge} grading in the p region results in a spatial variation in the CB energy of H4 as compared with that of H1, inducing in H4 a quasi-drift electric field in the SiGe region which accelerates electrons towards the end of this region [20]. A Ge grading from 0% to 30% over 400 nm theoretically produces a field of 6.5 kV cm^{-1} [21, 22].

Hence, the first set of structures (from H1 to H3) allows comparison among heterojunctions with a scaling in the integrated Ge concentration while at the same time keeping an identical box Ge profile and layer thickness. Structures H2 and H4 yield the comparison of two different Ge profiles having the same Ge equivalent thermodynamic stability point, as defined by Matthews and Blakeslee [23]: the integrated Ge concentration across the p region is held constant as the Ge profile shape is changed.

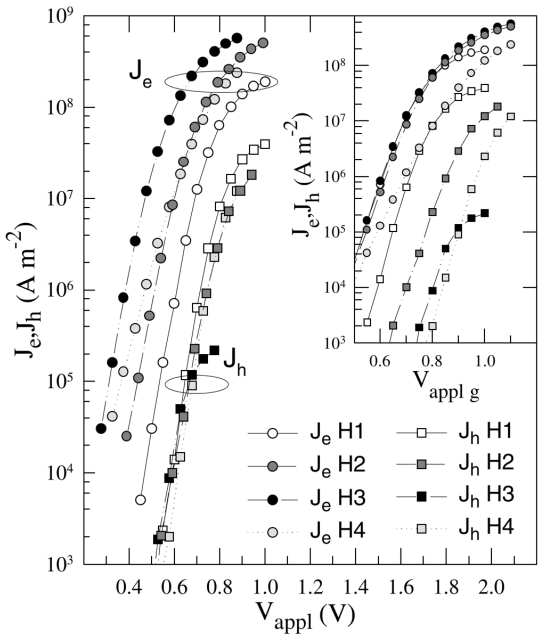

Figure 2. J_e, J_h–V_{appl} characteristics for the homostructure, the Ge box profile and Ge graded heterostructures. The J_e, J_h–$V_{appl\,g}$ characteristics (see text) are shown in the inset.

3. Average magnitudes of interest

Figure 2 shows the electron current density, J_e, and hole current density, J_h, of all the structures versus the forward applied voltage (V_{appl}). At this point it is necessary to stress that to obtain a given J_e, the abrupt Si/SiGe heterojunctions require a V_{appl} lower than that of the pure Si homojunction. The built-in voltage, V_{bk}, of a heterojunction is lower than that of Si homojunctions (with identical doping characteristics), as a result of the lower-bandgap material of the SiGe [22, 24]. The subscript k indicates the numbering of the heterostructures. Neglecting the small ΔE_c and the slight difference between the effective density of states of Si and SiGe, the difference between the built-in voltage of each heterostructure and the homostructure would be nearly equal to ΔE_{vk}.

Under low-injection conditions the dependence of the currents on applied voltage follow an exponential dependence according to a *barrier-controlled regime*. In H2 and H3 the reduction in the band-gap of SiGe as compared with that of Si reduces the barrier for electron injection into the SiGe region from the n^+ region (figure 1), leading to the above-mentioned increasing of J_e. This is called the 'heterojunction effect'. This effect essentially causes the ratio between the electron current density of the homojunction, $J_{e(Si)}$, and the one of the abrupt heterojunction, $J_{e(SiGe)}$ (while the holes maintain similar current densities), to increase exponentially with ΔE_G. The ratio between the electron current density in the homojunction and in the heterojunction can be expressed as [22, 25, 26]:

$$\frac{J_{e(SiGe)}}{J_{e(Si)}} = \frac{N_C N_{V(SiGe)}}{N_C N_{V(Si)}} \frac{\mu_{n(SiGe)}}{\mu_{n(Si)}} \exp\left(\frac{\Delta E_G}{k_B T}\right) = C_{(SiGe)} \exp\left(\frac{\Delta E_G}{k_B T}\right) \quad (1)$$

where $N_C N_{V(SiGe)}$ and $N_C N_{V(Si)}$ are the products of the effective density of states in the CB and the VB, and $\mu_{n(Si)}$ and $\mu_{n(SiGe)}$ are the carrier mobility in Si and SiGe. In this equation, the bulk recombination and the doping-induced bandgap narrowing (owing to the low doping levels) in the SiGe region have been neglected. The $C_{(SiGe)}$ factor in equation (1) can be easily extracted by fitting the $J_{e(SiGe)}/J_{e(Si)}$ characteristics obtained from the Monte Carlo simulation. For low x_{Ge}, $C_{(SiGe)}$ follows the ratio between low-field mobilities and the effective densities of states (equation (1)). However, when x_{Ge} increases, $C_{(SiGe)}$ no longer follows this simple ratio. Beyond the impact of x_{Ge} on the electron low-field mobility value, our Monte Carlo results clearly show that the pre-exponential factor, $C_{(SiGe)}$, in equation (1) no longer agrees with a simplistic picture (*drift diffusion*) of transport as x_{Ge} increases. Therefore, we should stress that the mobility ratio in equation (1) of our manuscript *is not* a simple ratio of low-field mobilities in Si and in SiGe, and it must take into account the complexity of transport in the structure (carrier heating, etc) [16].

The consequences of the spatial variation of the CB in a graded heterojunction, H4, are easily noticed in figure 2. The dependence on V_{appl} under *low-injection conditions* of J_e in H4 is modified: J_e does not follow the slope of 60 mV per decade at room temperature typical of a *pure barrier-controlled regime* found in H1, H2 and H3, whereas J_h continues to show such a dependence. A decrease in the slope of J_e appears as V_{appl} increases. This effect was emphasized by Crabbé *et al* in 1993 [27] and is the so-called 'Ge-ramp effect'. For H2 and H3 with a flat germanium profile, the movement of the edge of the space charge region in the p region typically has a small effect on J_e. However, the effect is magnified in a graded heterojunction due to the exponential dependence of J_e on the Ge content at that point.

Our main purpose in this work is to determine the microscopic noise sources and the effect of the Ge profile on noise characteristics. From this point of view, analysing the heterostructures for a given J_e under *low-injection conditions* for all the structures has certain advantages. With this aim, a translation of the J_e, J_h–V_{appl} characteristics of each heterostructure was made towards higher values of V_{appl}, (for each heterostructure (named k). J_e, J_h are plotted versus a 'generalized V_{appl} voltage': $V_{appl\,g} = V_{appl} + V_{b1} - V_{bk}$). The outcome can be observed in the inset in figure 2. For H4, the shift of the J_e, J_h characteristics towards higher voltages was done by taking $V_{b4} = V_{b3}$. Study of current fluctuations in bipolar devices [10–12] shows that the high-frequency noise is strongly related to the current density of the majority carriers of the higher-doping-density region (electrons in the present case) of these particular devices. Hence the total current fluctuations can be readily analysed and compared when using $V_{appl\,g}$ as a reference.

3.1. Low-injection regime

In order to make a bias-dependent estimation of the different transport properties involved in the abrupt and graded heterojunctions, the spatial dependence of different physical magnitudes was analysed. Figures 3(a), (b) and (c) plot the spatial dependence of the electron and hole concentrations,

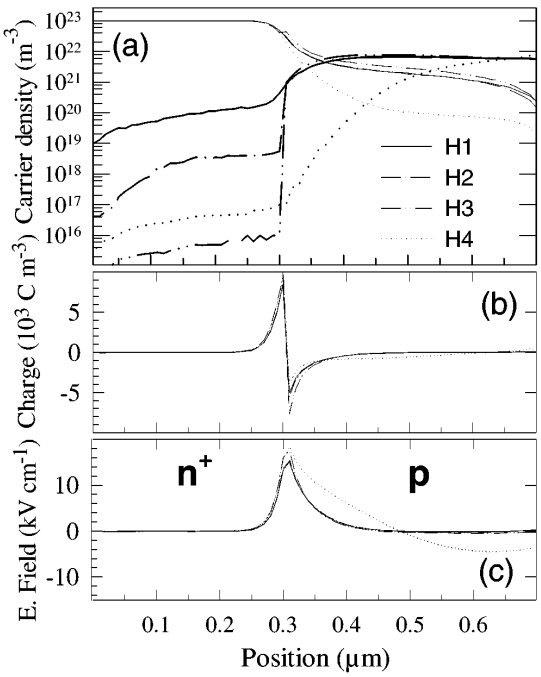

Figure 3. Comparison of electron (thin lines) and hole (thick lines) concentrations (a), spatial distribution of charge density (b) and electric field (c) in the four heterostructures for a given $V_{appl\,g}$ voltage equal to 0.65 V (*low-injection regime*).

the charge density and the electric field as a function of position for a $V_{appl\,g} = 0.65$ V (under *low-injection conditions*) for all the structures.

Figure 3(a) shows that the dominant effect on comparing H1 and H2 or H3 is the efficient blockade of holes originated by ΔE_v, inducing a negligible population of holes in the n^+ region (a hole concentration lower than 10^{19} m^{-3} or 10^{16} m^{-3} for H2 and H3, respectively). In contrast, due to the high doping density of this region (10^{23} m^{-3}), the charge dipole in H2 and H3 exhibits identical spatial dependence and is constituted by the same components as in H1: ionized impurity and a free electron layer in the SiGe region and ionized impurity in the Si region (figure 3(b)). Under these conditions, the electric field at the interface offers resistance to electron transport, thus justifying the exponential behaviour typical of a 'barrier-limited regime' of J_e in H2 and H3 (figures 2 and 3(c)).

J_e in H4 mainly follows two different types of behaviour, which we will classify as the *low-* and *extremely-high-injection regimes* of abrupt heterojunctions due to their noise behaviour, discussed below. Accordingly, for $V_{appl\,g} = 0.65$ V in H4 the gradual barrier of the SiGe VB results in a reduced presence of holes in the p region (insufficient to compensate the charge of the ionized impurities). This effect, combined with the electron transport enhanced by the quasi-drift electric field (figure 3(c)), yields both a reduction in the electron concentration in the SiGe layer as compared with that of H1 (figure 3(a)) and an extension of a 'non-neutral' region towards the ohmic contact of the p region unlike the results obtained for H1, H2 and H3 (figure 3(b)).

3.2. High-injection regime

By increasing voltage ($V_{appl\,g} > 0.75$ V), at the onset of the *high-injection regime* in the p region, ΔE_v begins to play an important role in the Ge box-profile heterojunctions (H2 and H3). The holes cannot surpass ΔE_v whereas the electrons easily cross the interface, resulting in a progressive accumulation of holes in the SiGe layer up to a point where the hole density begins to attract electrons to ensure charge neutrality (figure 4(a)). Moreover, the accumulation of electrons and holes makes the carrier density in the SiGe region comparable to the doping density of electrons in the n^+ region. Consequently, a reduction in the spatial extension of the charge dipole at the junction and a strong decrease in the maximum electric field take place (figures 4(c),(d)). For brevity, we only show the results for H3. The impact on the electron current density–voltage characteristics is that J_e begins to deviate (by a shift up) in H2 and H3 as compared with H1 (more pronounced when x_{Ge} increases) (figure 2, inset). This effect will have strong consequences on the noise of the Ge box-profile heterojunctions in this bias regime.

3.3. Extremely-high-injection regime

For abrupt heterojunctions, when going deeper into the *high-injection regime* the above commented strong accumulation of both types of carrier in the p region leads to an electron concentration larger than the impurity doping of the n^+ region. The fact that the continuity of the electron density at the interface is achieved elicits a change in the polarity of the charge dipole at the junction that now becomes exclusively established by free carriers (electrons and holes at the n^+ and p regions, respectively). The evolution of this phenomenon with bias can be observed in figure 4(b). Therefore, for $V_{appl\,g}$ above 0.85 V, the electric field at the junction has a positive peak. For $V_{appl\,g}$ higher than 0.90 V, a certain degree of current saturation can be observed in the J_e–$V_{appl\,g}$ characteristics of H2 and H3 (also present in H1 for lower $V_{appl\,g}$ values, figure 2).

In H4, when $V_{appl\,g}$ increases, the difficulty encountered by the holes in crossing the SiGe region is reduced and hence the free hole density begins to draw close to the doping profile in an increasingly larger part of the p region (figure 4(a)). Accordingly, it expands the region in which the built-in field is constant and its value is in agreement with the estimated field arising from the variation at the CB edge (figure 4(e)). Furthermore, for the highest values of $V_{appl\,g}$, the charge dipole begins to fill a narrower region closer to the junction (figure 4(d)) in the same way as in H1 for the *low-injection regime* (figure 3(b)). As discussed below, this phenomenon has a strong effect on the noise characteristics of H4.

4. Comparative study of current fluctuations

4.1. Theoretical aspects

Since our aim is to analyse the effect of the different Ge profiles on the noise characteristics of the heterostructures under study, prior to offering the results on noise we briefly describe a theoretical analysis of noise as adapted to the existing situation. To study current fluctuations in the

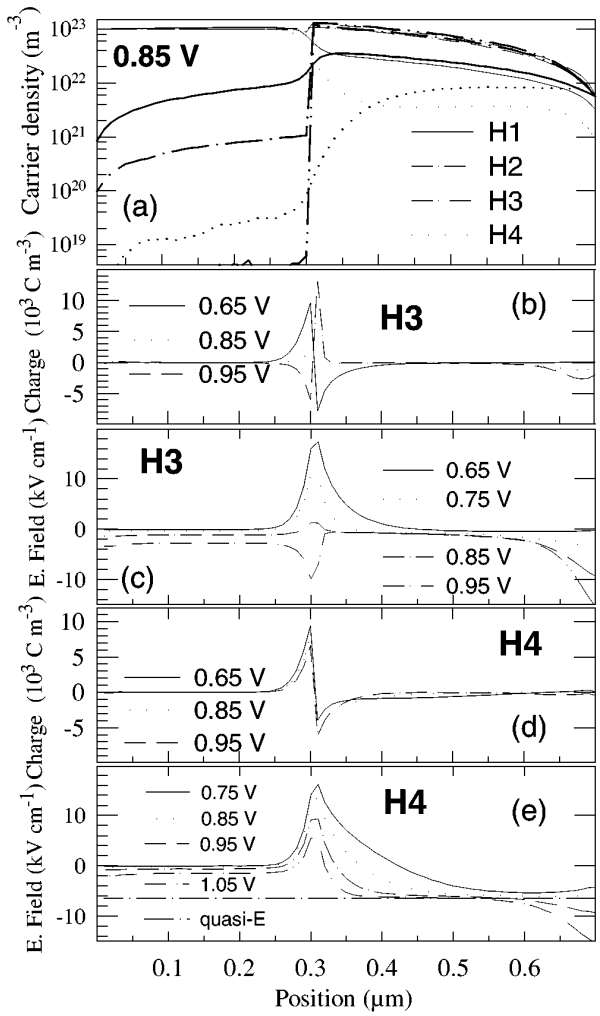

Figure 4. Electron (thin lines) and hole (thick lines) concentrations for $V_{appl\,g} = 0.85$ V, (a). Comparison of spatial distribution of charge density, (b) and (d) and electric field, (c) and (e), in the abrupt heterojunction with the largest Ge content (30%), H3, and the graded heterojunction, H4, for different bias conditions including *low-* and *high-injection-voltage regimes*.

current-noise operation mode, the current must be allowed to fluctuate while the voltage applied to the electrodes is kept constant [28]. The spectral density of total current fluctuations, $S_J(f)$, is the mathematical magnitude required for characterizing the current noise over a given frequency range. The analysis used to calculate the current fluctuations has been addressed in depth for 1D bipolar structures in earlier works [10, 12]. The method allows one to express $S_J(f)$ by means of the terms associated with the electron and hole current fluctuations, respectively, $S_{Je}(f)$ and $S_{Jh}(f)$, and the cross-correlation between electron and hole current fluctuations $S_{Jc}(f)$:

$$S_J(f) = S_{Je}(f) + S_{Jh}(f) + S_{Jc}(f). \qquad (2)$$

Since immediate comparison of S_{Je}, S_{Jh}, S_{Jc} among different structures does not furnish direct conclusions, a spatial analysis of noise for these SiGe/Si heterostructures based on the spatial J_e and J_h calculation is required [12]. Hence, S_{Je} is given by

$$S_{Je}(f) = S_{Je}^{pp}(f) + S_{Je}^{n^+n^+}(f) + S_{Je}^{pn^+}(f) + S_{Je}^{n^+p}(f) \qquad (3)$$

where $S_{Je}^{pp}(f)$ and $S_{Je}^{n^+n^+}(f)$ are the spectral densities of the J_e fluctuations in the p and n$^+$ regions, respectively. $S_{Je}^{pn^+}(f)$ and $S_{Je}^{n^+p}(f)$ are the terms related to the cross-correlation of J_e fluctuations between both regions of the devices. An identical treatment can be applied to $S_{Jh}(f)$ and $S_{Jc}(f)$. The spatially restricted $S_{Je}(f)$, $S_{Jc}(f)$ and $S_{Jh}(f)$ allow one to determine the effect of the Ge content in H2–H3 and the graded Ge profile in H4 on $S_J(f)$.

It is important to mention here that current fluctuations can be originated by fluctuations in velocity and/or in carrier number. In all the structures considered here, an extinction of carrier number fluctuations due to the long-range Coulomb interaction was observed [29]. Therefore, $S_J(f)$ is only determined by the contribution of velocity fluctuations, in which the mean number of particles acts as a weighting factor [10, 12, 29].

4.2. Spectral density of total current density fluctuations: $S_J(f)$.

By using this mathematical approach we begin our comparative analysis of noise characteristics for the heterojunctions based on the previous physical study of each structure. Figure 5 shows $S_J(f)$ for all the heterojunctions and several $V_{appl\,g}$ conditions.

A detailed discussion of $S_J(f)$ in H1 may be found elsewhere [10]. When carefully scrutinizing the results on the $S_J(f)$ of H1 one sees that it displays three different ranges of behaviour, depending on $V_{appl\,g}$. For voltages up to the built-in potential, $S_J(f)$ exhibits a maximum (around 1200 GHz) and its amplitude and frequency remain almost constant within this bias range. As bias increases, the frequency of the maximum is steadily reduced. A significant increase in $S_J(0)$ can also be observed for the highest bias conditions.

On comparing the $S_J(f)$ results of the Ge box-profile heterojunctions with the results for H1 in figure 5, one observes frequency-dependent peculiarities given by the introduction of an SiGe layer in the p region; these peculiarities are strongly altered as x_{Ge} increases. As the main remarkable effect, $S_J(f)$ increases sharply in the 0–1000 GHz range for a given $V_{appl\,g}$. For $V_{appl\,g} > 0.90$ V, a pronounced maximum located at very high values of frequency (2500–3000 GHz) sets in, together with an additional increase in $S_J(0)$. However, if one analyses the $V_{appl\,g}$ dependence of $S_J(f)$ in H2 and H3, one again identifies the three different ranges observed in H1, with additional features as follows: In the *low-injection regime* of the SiGe region ($V_{appl\,g} \leqslant 0.75$ V), the noise performance of H2 and H3 remains identical to the one found in H1. When the diode operates in the *high-injection regime* for the p-SiGe region, the $S_J(f)$ maximum seen in figures 5(b), 5(c) for the previous range is no longer present. In contrast, a new and intense maximum located at lower frequencies is established, which leads to a rise in $S_J(0)$.

In the Ge graded heterojunction, H4, when the comparison is made with H1, a strong reduction in $S_J(0)$

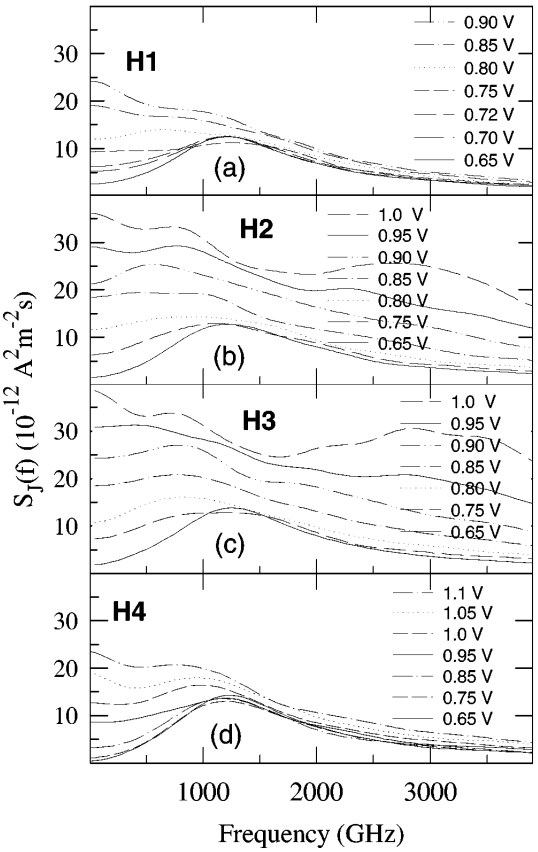

Figure 5. Spectral density of current fluctuations, $S_J(f)$, for the homojunction H1 (a), the abrupt heterojunction (Ge box profile) and $x_{Ge} = 0.15$ H2 (b), the abrupt heterojunction and $x_{Ge} = 0.30$ H3 (c) and the graded heterojunction H4 (d), for several $V_{appl\,g}$.

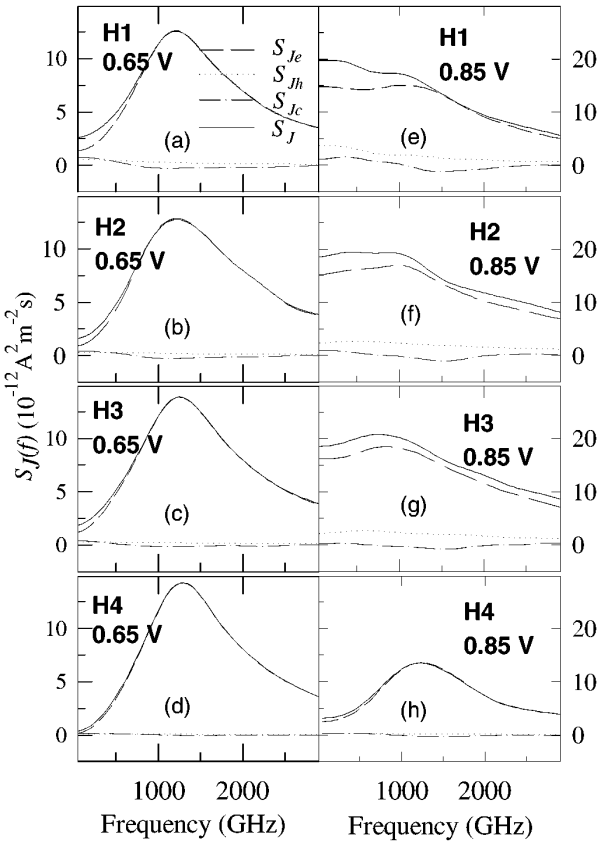

Figure 6. Decomposition of $S_J(f)$ into the $S_{Je}(f)$, $S_{Jh}(f)$ and $S_{Jc}(f)$ terms as indicated in equation (2). A bias $V_{appl\,g} = 0.65$ V is depicted in figures 6(a) (H1), 6(b) (H2), 6(c) (H3) and 6(d) (H4). A bias in the *high-injection regime* in the SiGe layer ($V_{appl\,g} = 0.85$ V) is plotted in figures 6(e) (H1), 6(f) (H2), 6(g) (H3) and 6(h) (H4).

is found for the same value of $V_{appl\,g}$. Additionally, figure 5 reveals that the dependence of $S_J(f)$ on frequency for different $V_{appl\,g}$ values is quantitatively similar to that occurring in H1 if one performs a downshift (around 0.22 V) in the values of $V_{appl\,g}$, or, in simpler terms, if one compares the situation with what happens for V_{appl}. Hence, the frequency and the $V_{appl\,g}$ dependence of the $S_J(f)$ characteristics of H1 and H4 remain comparable while J_e in H4 is strongly enhanced.

In figure 5 it is interesting to compare the structures which have the same total Ge content: H2 and H4. At this point one finds an advantageous reduction of $S_J(f)$ in H4 in comparison with the one calculated for H2 for a given $V_{appl\,g}$. The decrease in $S_J(0)$ in H4 is especially remarkable. This is exclusively linked to the Ge grading and therefore the absence of ΔE_v in H4.

4.3. High-frequency behaviour of $S_{Je}(f)$, $S_{Jh}(f)$ and $S_{Je}(f)$

Below, an in-depth investigation (based on the average magnitudes of the heterojunctions) is offered to determine how the Ge content and band discontinuities modify J_e and J_h fluctuations. We begin by performing the initial decomposition of $S_J(f)$ into the $S_{Je}(f)$, $S_{Jh}(f)$ and $S_{Jc}(f)$ terms, as shown in figure 6.

4.3.1. Low-injection regime. A detailed discussion of $S_J(f)$ in H1 has been already published [10] and the main features are only summarized for comparative purposes. Regarding the high-frequency dependence, $S_J(f)$ is governed by the highly doped region (n^+). Hence, $S_J(f)$ is dominated by $S_{Je}(f)$ and displays a peak up to values of 13×10^{-12} A^2 m^{-2} s (at a frequency close to 1200 GHz), which is related to the plasma frequency of electrons in the n^+ region. Figures 6(b)–6(d) demonstrate that $S_{Je}(f)$ mainly determines $S_J(f)$ in the heterostructures in the same way as occurs in H1, confirming that the SiGe layer in the p region has no significant effect on noise at low injection.

4.3.2. High-injection regime in the SiGe layer. In H1, when $V_{appl\,g}$ increases (figure 6(e)) the frequency of the $S_{Je}(f)$ maximum at 1200 GHz undergoes no deviations with respect to the *low-current regime*, mainly due to the identical charge conditions. Hence, the displacement of the $S_J(f)$ maximum towards lower frequency values in H1 (shown in figure 5) is related to the increasing importance of the hole component, $S_{Jh}(f)$, for frequencies below 1500 GHz.

Bearing in mind that at the start of the *high-injection regime* ΔE_v begins to enhance J_e, one would expect a modified noise response in H2 and H3. Figures 6(f) and 6(g) illustrate an increase in $S_J(f)$ in the 0–1000 GHz range that

is not related to an increase in $S_{Jh}(f)$ (as occurs in H1) but rather to a downshift in the frequency of the $S_{Je}(f)$ maximum in H2 and H3 that is slightly dependent on the Ge content (as x_{Ge} increases from 0 to 0.30, it varies from 1200 GHz to 850 GHz). Accordingly, the major peculiarity in noise characteristics is yielded by the electron component, $S_{Je}(f)$, degrading the noise characteristics. To analyse this special effect it is appropriate to perform a spatial analysis of the $S_{Je}(f)$ term, which is addressed in the next section. Moreover, an identical $S_{Jh}(f)$ component (which has been confirmed to come entirely from the SiGe region) in H1, H2 and H3 is found (figures 6(e), (f), (g)). This indicates that in spite of the strong accumulation of holes in the SiGe layer (figure 4(a)), the reduction of the hole current due to the valence band discontinuity (ΔE_{Vk}) gives rise to lower hole current density fluctuations in that region.

With identical reasoning for the graded heterojunction, H4, figure 6(h) shows that for $V_{appl\,g} = 0.85$ V the noise behaviour is maintained within the *barrier-limited current regime* due to the slow accumulation of carriers in the SiGe layer when bias increases. Moreover, for voltages as high as 0.85 V, by using a grading of Ge in the p region the influence of the majority carriers in the SiGe layer on $S_J(f)$ becomes negligible.

4.3.3. Spatial study of current fluctuations: high- and extremely-high-injection regimes. In order to illustrate the origin of the noise characteristics in these regimes, it is useful to observe the evolution of the spatial terms that determine $S_{Je}(f)$ with $V_{appl\,g}$ in the different regions of the abrupt structures. Since the effects observed in abrupt heterojunctions are more remarkable as x_{Ge} increases, for brevity only the H3 case has been included in our spatial study ($V_{appl\,g} = 0.85$ V and 0.95 V, figure 7). This figure also shows these terms for $V_{appl\,g} = 1.1$ V in H4. It should be stressed that in H1 (figure 6(e)), $S_{Je}(f)$ is essentially built by the $S_{Je}^{n^+n^+}(f)$ term.

For $V_{appl\,g} = 0.85$ V and 0.95 V in H3, figures 7(a), (c) display an increase in $S_J(f)$ in the 0–1000 GHz range only associated with $S_{Je}(f)$. From figures 7(b), (d) (which show the spatial components of $S_{Je}(f)$ of figure 7(a), (c), respectively), it can be seen that the variation in $S_{Je}(f)$ is not supported by a single term but it is built by the contributions to the J_e fluctuations across whole device. A first issue is that the significant change in $S_{Je}(f)$ as bias increases is mainly caused by the low frequency increase in $S_{Je}^{pp}(0)$, which is associated with the heating of electrons in the SiGe region (see electric field, figure 4(c)). This effect is present in H1 but it is amplified in the heterojunctions due to the large accumulation of electrons in the SiGe layer originated by ΔE_v. Furthermore, a second result arises from the positive electric field: when bias increases, this field helps the correlation of J_e fluctuations between the p and the n regions, exacerbating the importance of the $S_{Je}^{pn^+}(f)$ and $S_{Je}^{n^+p}(f)$ terms between 0 and 1000 GHz. For the largest $V_{appl\,g}$, a low frequency increase in the $S_{Je}^{n^+n^+}(f)$ component is also detected due to a non-negligible electric field in the quasi-neutral n^+ region (figure 4(c)). In general, all these issues are related to the loss of preponderance of the highly doped (n^+) region (figures 7(b), (d)) as a consequence of the progressive accumulation of electrons in the SiGe layer and the reduction in the space charge region.

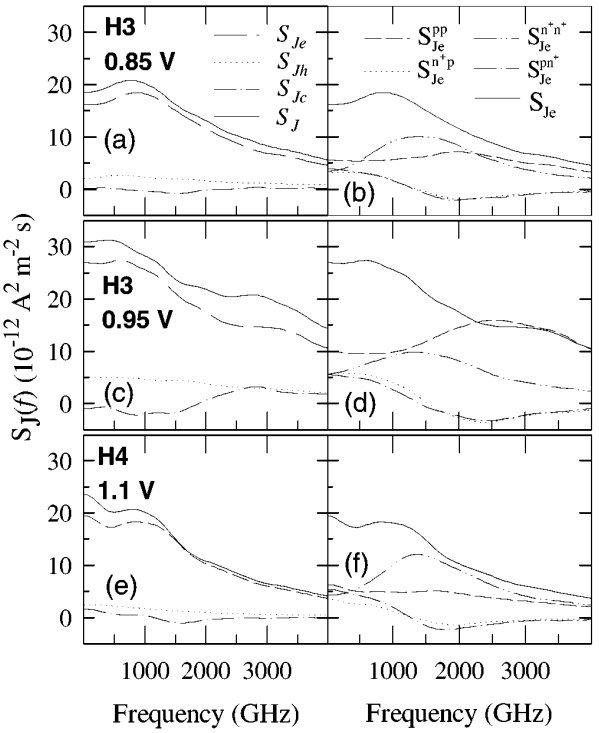

Figure 7. Different terms contributing to the spectral density of current fluctuations, $S_J(f)$, as indicated in equation (3), in H3 for two bias conditions: (a) 0.85 V in *high-injection regime* and (c) 0.95 V in *extremely-high-injection regime*. In H4 for 1.1 V (e). Spatial contributions to $S_{Je}(f)$: $S_{Je}^{pp}(f)$, $S_{Je}^{n^+p}(f)$, $S_{Je}^{pn^+}(f)$ and $S_{Je}^{n^+n^+}(f)$ related to the left voltage conditions in H3, (b) and (d), and H4, (f). In (b), (d) and (f), the superindex in S_{Je} indicates the regions (n^+ or p) involved in the calculation of the current correlations.

In H3 an additional effect throughout the frequency range for extremely high conditions is the increased importance of $S_{Je}^{pp}(f)$ to the detriment of $S_{Je}^{n^+n^+}(f)$. Let us study the origin of the significant increase in $S_J(f)$ in the 2500–3000 GHz range for $V_{appl\,g}$ above 0.90 V. This additional maximum is associated with $S_{Je}(f)$ and $S_{Jc}(f)$ (figure 7(c)). Using a spatial analysis of noise for 0.95 V (figure 7(d)), one determines the origin of the $S_{Je}(f)$ relative maximum as the increase in $S_{Je}^{pp}(f)$ at 2500 GHz. For the highest $V_{appl\,g}$ values, the carrier concentration in the SiGe region reaches and exceeds the doping density of the n^+ region (figure 3(c)), leading to considerable J_e fluctuations in the SiGe layer: $S_{Je}^{pp}(f)$.

As commented, the *extremely-high-frequency regime* effects in H4 are 'calmed down' to a considerable extent by the Ge grading. Figures 7(e), (f) show that the noise characteristics in this structure coincide with those of the homojunction when a given V_{appl} is considered. The peak of $S_{Je}^{n^+n^+}(f)$ continues to show a value around 13×10^{-12} A^2 m^{-2} s at 1200 GHz, indicating the preponderance of the n^+ region in the high-frequency noise in H4.

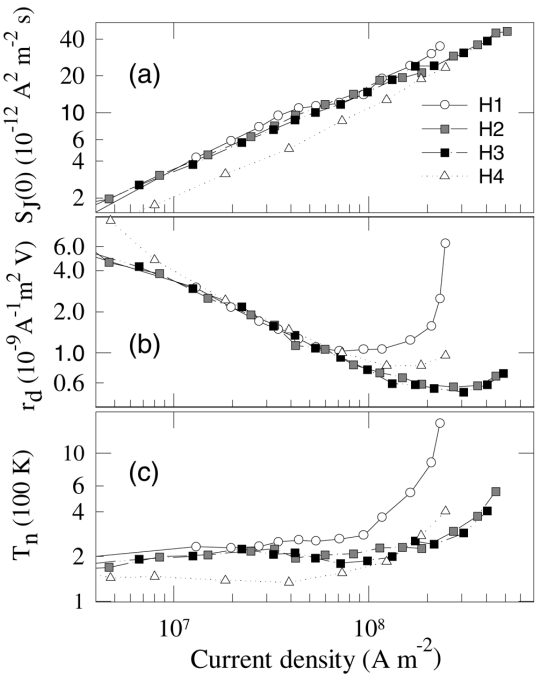

Figure 8. The low-frequency value of the spectral density of total current density fluctuations, $S_J(0)$, is depicted together with the differential resistance of the structure, r_d, and the low-frequency noise temperature, T_n, as a function of the current density for the homostructure, the box-profile heterostructures and the graded heterostructure.

4.4. Low-frequency noise

Our model excludes generation–recombination mechanisms responsible for burst and flicker noise. Those mechanisms determine $S_J(0)$ in a real device for low frequencies. Bearing this in mind, our results are valid for frequencies above the *corner frequency* of the device (typically, in the 100 kHz–10 MHz range). In other words, the calculated low-frequency values of magnitudes such as $S_J(f)$ are to be considered as RF values (0.5 GHz–10 GHz). The dependence of equivalent noise temperature at low frequencies, T_n, on the structures can be understood in terms of the behaviour of $S_J(0)$ and the differential resistance of the structures, r_d. Figures 8(a), (b) and (c) depict $S_J(0)$, r_d and T_n, respectively, of all the heterojunctions as a function of current density [8]. From the r_d plot, the three different regimes of J_e–$V_{appl\,g}$ commented on in previous sections can easily be distinguished.

When studying the Ge box-profile heterojunctions, H2 and H3, at *low-injection conditions*, the values of J_e for a given $V_{appl\,g}$ coincide with those of H1 and hence r_d does not exhibit any remarkable dependence on x_{Ge} (from 0 to 0.30). As J_e decreases in this range, some reduction in T_n is found in the Ge box heterojunctions due to the lower weight of $S_J(0)$. However, the deviation of the J_e slope on H2 and H3 from the H1 one into the second regime induces a continuous decrease in r_d (up to current values of 2×10^8 A m^{-2}) marking the end of the *high-injection regime* of the abrupt heterojunctions. Despite the increase in $S_J(0)$ in this regime, the decrease in r_d is more marked, forcing T_n to exhibit a local minimum (more outstanding as the Ge content increases) at around 7–9 $\times$ 10^7 A m^{-2}. This indicates the existence of an optimum T_n value within this regime. When going deeper into the *extremely-high-injection regime*, the moderate increase in r_d agrees with the already observed saturation of J_e, determining larger values of T_n, which reaches a maximum of 500 K. The reduction in noise temperature for larger J_e values is comparable in H2 and H3. The lack of dependence on x_{Ge} indicates that this reduction is merely determined by the heterojunction presence. Throughout the current density range, the box-profile heterojunction diodes exhibit lower T_n values as compared to those of H1.

Due to the Ge grading in H4, *the low-injection conditions* extend to currents up to 7 $\times$ 10^7 A m^{-2}. Therefore, at this point we can draw important conclusions about H4: First, the $S_{Je}(0)$ and $S_{Jh}(0)$ components of $S_J(0)$ undergo a pronounced reduction linked to the observed quasi-electric field drift and the depletion of holes in the p region (figures 3(a), 4(a), 5(d) and 8(a)). Second, in the current density range shown in figure 8(b), despite the current 'roll-off' effect, the r_d–J_e characteristic is comparable to that of the homojunction (figure 2 inset). As a consequence of these effects, a very low value of T_n (lower than the lattice temperature) is found across almost the whole density current range. This result is in agreement with the barrier-limited transport demonstrated in figure 4(e). For current density values larger than 7 $\times$ 10^7 A m^{-2}, $S_J(0)$ continues to show a constant increase while J_e exhibits a dependence typical of quasi-saturation. In H4, r_d takes intermediate values between the ones observed for H1 and for H2–H3. Hence, in this regime, an increase in T_n in H4 occurs and, for a given J_e, this magnitude reaches lower values than in the homojunction but larger ones than those seen for the abrupt heterojunctions.

5. Summary

A novel one-dimensional Monte Carlo study dealing with Ge profile considerations for current-mode analysis of n-Si/p-$Si_{1-x}Ge_x$ heterojunctions has been presented. Two different Ge profiles across the p region have been considered: box (for different x_{Ge}) and triangular. We focus on the alterations in stationary carrier transport as well as on the microscopic origin of the low- and high-frequency noise through different aspects such as transport in the pseudomorphic SiGe layer, valence and conduction band discontinuities and the electric field arising due to the Ge grading. Three different voltage-dependent operation regimes have been observed to appear in the structures, which have been called low-, high- and extremely-high-injection conditions.

Under low-injection conditions, the presence of a constant Ge percentage strongly enhances J_e due to the Ge-induced bandgap narrowing of the SiGe layer (more pronounced with the increase in x_{Ge}). Only a lower $S_J(0)$ value due to a small weight of $S_{Jh}(f)$ (associated with the scarcity of holes in the SiGe layer) is emphasized because it results in a slight decrease in T_n within this range, independent of x_{Ge}.

At the start of the high-injection regime in the SiGe layer, J_e begins to deviate in the box-profile heterojunctions as compared with the situation in the homojunction. This behaviour is related to the control of the carrier distribution by ΔE_v. The $S_J(f)$ of abrupt heterojunctions is strongly degraded in the 0–1000 GHz range. Based on the spatial analysis, we identified the origin of the maximum located in this range as being related to the increase in $S_{J_e}^{pp}(0)$. This reflects electron heating in the p region, which is amplified in the heterojunctions as x_{Ge} increases. Also, the reduction in the negative electric field helps the correlation of J_e fluctuations between the n and the p region, affording extra importance to the total $S_{J_e}(f)$ term. For a given J_C current in this region, a continuous decrease in the differential resistance forces T_n to exhibit a local minimum (more outstanding as x_{Ge} increases).

Beyond the high-injection regime, a certain degree of current saturation can be observed in the J_e–$V_{appl\,g}$ characteristics of the abrupt heterojunctions, together with the consequent increase in r_d. An additional maximum of $S_J(f)$ located at very high frequency values (2500–3000 GHz) is established. Its origin is related to the fact that the carrier concentration in the p region exceeds the doping density of the n^+ region. Regarding the low-frequency behaviour, the increase in r_d determines larger values of T_n (almost independent of x_{Ge}) as compared with the previous range, but always lower than those of the homojunction for a given J_e.

The Ge grading produces a reasonable enhancement in J_e as well as better noise characteristics in comparison with the abrupt heterojunctions. The bias and the frequency dependence of $S_J(f)$ are similar to those found in the homojunction. In H4, due to the helping field to the electron transport in the SiGe layer, the *low-injection conditions* extend to currents up to 7×10^7 A m^{-2} (the slope of J_e being characterized by the 'Ge-ramp' effect). However, the hole contribution to noise is efficiently removed, yielding a very low value of T_n. For the highest current values an increase in T_n is seen, which reaches higher values than in the abrupt heterojunctions.

Acknowledgments

This work has been funded by research project PB97-1331 from the Dirección General de Enseñanza Superior e Investigación Científica and by research project SA44/99 from the Junta de Castilla y León.

References

[1] Harame D L, Comfort J H, Cressler J D, Crabbé E F, Sun J Y-C, Meyerson B S and Tice T 1995 *IEEE Trans. Electron Devices* **42** 469
[2] Vook D *et al* 1994 *IEEE Trans. Electron Devices* **41** 1013
[3] Kasper E, Kibbel H, Herzog H and Gruhle A 1994 *Japan. J. Appl. Phys.* **33** 2415
[4] Schumacher H, Erben U and Gruhle A 1994 *Proc. IEEE Microwave Millimeter-Wave Circuit Symp. Dig. (San Diego, CA)* p 213
[5] Cressler J D 1998 *IEEE Trans. Microwave Theory Tech.* **46** 572
[6] Jacoboni C and Reggiani L 1983 *Rev. Mod. Phys.* **55** 645
[7] Hinckley J M and Singh J 1996 *J. Appl. Phys.* **80** 6766
[8] Varani L, Reggiani L, Kuhn T, Gonzalez T and Pardo D 1994 *IEEE Trans. Electron Devices* **41** 1916
[9] Gonzalez T, Pardo D, Varani L and Reggiani L 1995 *IEEE Trans. Electron Devices* **42** 1991
[10] Martín M J, Velázquez J E and Pardo D 1996 *J. Appl. Phys.* **79** 6975
[11] Martín M J, Pardo D and Velázquez J E 1997 *Phys. Status Solidi* b **204** 462
[12] Martín-Martínez M J, Pardo D and Velázquez J E 1998 *J. Appl. Phys.* **84** 5012
[13] Roulston D J 1990 *Bipolar Semiconductor Devices* (New York: McGraw-Hill)
[14] Martín M J, González T, Velázquez J E and Pardo D 1993 *Semicond. Sci. Technol.* **8** 1291
[15] People R and Bean J C 1985 *Appl. Phys. Lett.* **47** 322
[16] Moglestue C 1993 *Monte Carlo Simulation of Semiconductor Devices* (London: Chapman and Hall)
[17] van de Valle C G and Martin R M 1986 *Phys. Rev.* B **34** 5621
[18] Jain S C, Poortmans J, Iyer S S, Loferski J J, Nijs J, Mertens R and Van Overstraten R 1993 *IEEE Trans. Electron Devices* **12** 2338
[19] Laux S E and Fischetti M V 1991 *Monte Carlo Device Simulation: Full Band and Beyond* (Boston, MA: Kluwer)
[20] Kroemer H 1985 *Solid State Electron.* **28** 1101
[21] Hueting R J E 1997 Charge carrier transport in silicon–germanium heterojunction bipolar transistors *PhD Thesis* University of Delft
[22] King C A, Hoyt J L and Gibbons J F 1989 *IEEE Trans. Electron Devices* **36** 2093
[23] Matthews J W and Blakeslee A E 1974 *J. Cryst. Growth* **27** 118
[24] Chuang S L 1995 *Physics of Optoelectronic Devices* (New York: Wiley)
[25] Ashburn P, Boussetta H, Hashim M D R, Chantre A, Mouis M, Parker G J and Vincent G 1996 *IEEE Trans. Electron Devices* **43** 774–83
[26] Le Tron B, Hashim M D R, Ashburn P, Mouis M, Chantre A and Vincent G 1997 *IEEE Trans. Electron Devices* **44** 715
[27] Crabbé E F, Cressler J D, Patton G L, Stork J M C, Comfort J H and Sun J Y-C 1993 *IEEE Electron Device Lett.* **14** 193
[28] González T, Pardo D, Varani L and Reggiani L 1993 *Appl. Phys. Lett.* **63** 3040
[29] Varani L, Kuhn T, Reggiani L and Perlès Y 1993 *Solid State Electron.* **36** 251